



Effects of Sm and Y on the electron property of the anodic film on lead in sulfuric acid solution

D.G. Li*, J.D. Wang, D.R. Chen

State Key Laboratory of Tribology, Tsinghua University, Beijing 100084, China

HIGHLIGHTS

- The growth of PbO in the anodic film on lead electrode at 1.28 V in sulfuric acid was inhibited by the addition of Sm or Y.
- The passive capacity of lead electrode in sulfuric acid was improved by the addition of Sm or Y.
- The numbers of point defect in the anodic films on lead electrode at 1.28 V, 1.5 V and 1.8 V increase with increasing Sm or Y.

ARTICLE INFO

Article history:

Received 27 September 2012

Received in revised form

3 December 2012

Accepted 17 January 2013

Available online 31 January 2013

Keywords:

Lead alloy

Anodic film

Electrochemical impedance spectra (EIS)

Mott–Schottky plot

Rare earth element

ABSTRACT

The influences of Sm and Y on the electron properties of the anodic films on lead at 1.28 V(vs.SCE), 1.5 V(vs.SCE) and 1.8 V(vs.SCE) in 4.5 mol L^{−1} sulfuric acid are investigated by using electrochemical impedance spectroscopy (EIS), Mott–Schottky plot, galvanic polarization and photo-electrochemical technique. The results show that Sm and Y can significantly decrease the resistances of the anodic films on lead electrode at 1.28 V, 1.5 V and 1.8 V, the oxygen and hydrogen evolutions of lead electrode covered by the anodic film decrease with the addition of Sm or Y. The anodic films on lead electrode at three potentials appear an *n*-type semi-conductive character, the addition of Sm or Y can decrease the slope of M–S plot of the anodic film, it implying the increment of the defect density within the anodic film, which is beneficial for improving the charge–discharge behavior of the lead acid battery.

© 2013 Elsevier B.V. All rights reserved.

1. Introduction

In recent twenty years, lead–antimony alloy have been replaced by lead–calcium alloy as the choice of the positive materials in lead acid battery for its high corrosion rate, high water loss and even to self-discharge [1]. The hydrogen evolution potential of calcium is higher than that of antimony in sulfuric acid, accordingly the water loss of lead–calcium alloy sharply decreases, and then the lead–calcium alloy can become the candidate of the positive grid for the maintenance-free lead acid battery. While for lead–calcium alloy, a serious problem is the anodic film with high impedance (about 10¹⁰ Ω cm²) on its surface during charging and discharging, which is responsible for the so-called premature capacity loss “PCL” of lead acid battery [2–7]. The addition of Sn into lead–calcium alloy can effectively decrease the impedance of the anodic film by incorporated

into the PbO lattice [8] or decreasing the thickness of PbO film [2], but excessive Sn may lead self-discharge for lead acid battery [9,10].

To better solve the “PCL”, many rare earth elements such as Ce [11–13], Yb [14], La [15], Sm [16], Li [17] and Sr [18] are involved into lead–calcium–tin alloy, the results show that these rare earth elements can effectively decrease the resistance of the anodic film, and therefore the deep recycle property of the lead acid battery is improved. However, the above investigations are mainly focused on the electron property of the anodic film on lead alloy with or without rare earth element at 0.9 V (vs.Hg/Hg₂SO₄), and fewer papers report the rare earth element effect on the anodic films on lead alloy at the potentials above 0.9 V (vs.Hg/Hg₂SO₄). It is well known that the positive grid may be suffered from a large potential cycle during the factual operation, the anodic film formed at high potentials can affect the electron properties of the positive grid, and then to affect the application property of the lead acid battery. While up to now, there are no reports about this issue. The aim of this work is to determine the influences of Sm and Y on the electrochemical behaviors of the anodic films on lead–stannum

* Corresponding author. Tel.: +86 10 6279 5148; fax: +86 10 6278 1379.
E-mail address: dgli@mail.tsinghua.edu.cn (D.G. Li).

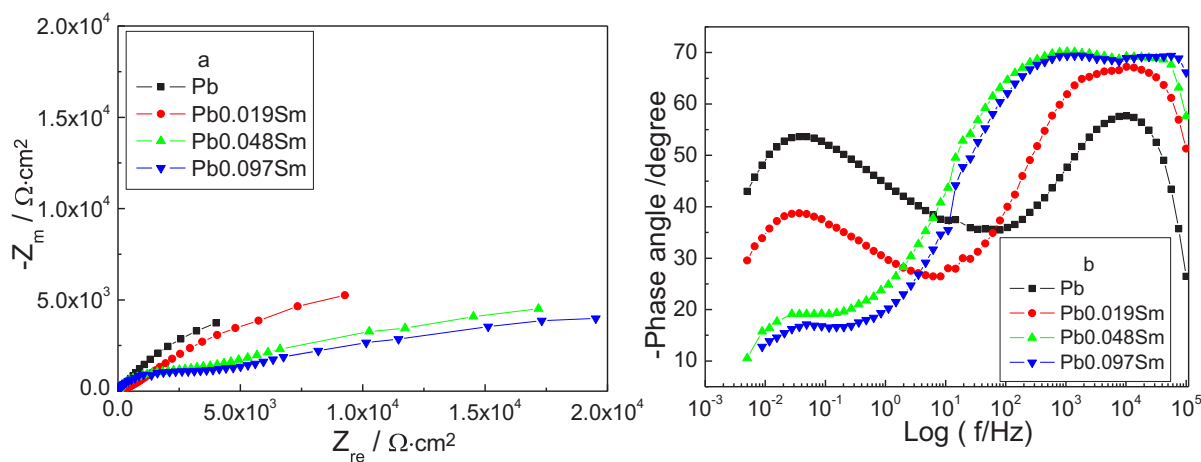


Fig. 1. EIS of the anodic films on Pb, Pb0.019%Sm, Pb0.048%Sm and Pb0.097%Sm alloys at 1.28 V for 3 h in 4.5 mol L⁻¹ H₂SO₄ solution, a) Nyquist plot; b) corresponding Bode phase angle.

and lead–yttrium alloys at 1.28 V(vs.SCE), 1.5 V(vs.SCE) and 1.8 V(vs.SCE) in 4.5 mol L⁻¹ H₂SO₄ solution.

2. Experimental

2.1. Material and sample

The experimental material is prepared by weighed mixture of pure lead (99.99 wt%), pure samarium (99.99 wt%) and pure yttrium (99.99 wt%) in an electric furnace with nitrogen as protect gas. Sm and Y are added into lead molten at 1000 K, after adequate stirring for 10 min. When the molten temperature drops to 723 K, the molten alloy is poured into a copper mold in the atmosphere to form the blank rod ($\Phi 20 \times 100$ mm), and the rod samples are machined in a form of wafer ($\Phi 10 \times 5$ mm). The compositions of the casting alloys are determined by chemical analysis, the result is listed as following: Pb, Pb0.019wt.%Sm, Pb0.048wt.% Sm, Pb0.097wt.% Sm, Pb0.018wt.%Y, Pb0.047wt.%Y and Pb0.095wt.%Y. One end surface of the sample exposed in the electrolyte acted as the working surface is abraded with 2000 grit SiC paper, polished with 0.5 μm Al₂O₃ powder and then cleaned using double-distilled

water, while other surfaces are sealed with epoxy resin in the lower part of an L-shaped glass tube.

2.2. Electrochemical experiments

All electrochemical experiments are performed in a conventional three-electrode cell, the counter and reference electrodes are a platinum mesh and SCE electrode, respectively. All potentials mentioned in this paper are referred as the reference electrode.

EIS apparatus is consisted of EG&G instrument model 273A electrochemical working station with 5210 frequency response analyzer, the potential is increased by 10 mV and the sweeping frequency is from 100 kHz to 5 mHz.

Mott–Schottky plots of the anodic films are also carried out at EG&G instrument model 273A electrochemical working station with a 10 mV s⁻¹ scanning rate, the scanning potential range is from 0 V to 2 V, and the measured frequency is 1000 Hz.

The photocurrent measurement is made of a conventional three electrode cell of 1-multi neck flash with a quartz window as a photon inlet, a 300W Xenon arc lamp is used as a light source, a monochromatic light with a wavelength from 200 nm to 800 nm is provided by a scanning digital monochromator controlled by a stepping

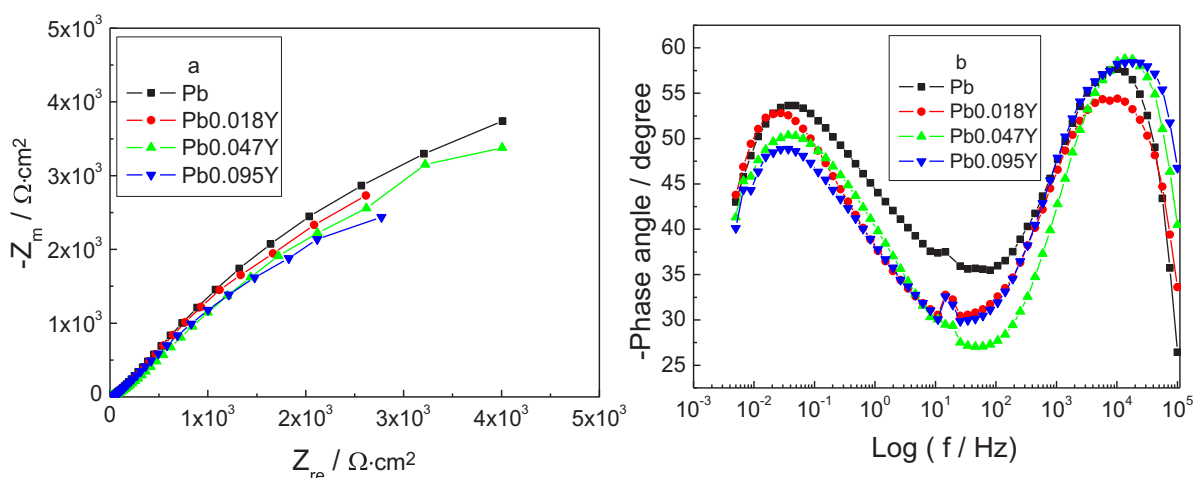


Fig. 2. EIS of the anodic films on Pb, Pb0.018Yt, Pb0.047Yt and Pb0.095Yt alloys at 1.28 V for 3 h in 4.5 mol L⁻¹ H₂SO₄ solution, a) Nyquist plot; b) corresponding Bode phase angle.

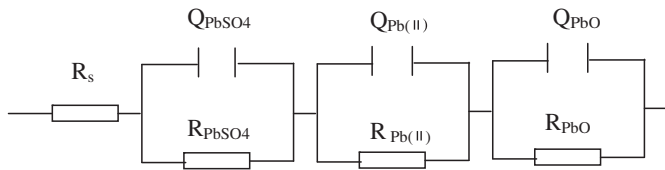


Fig. 3. The equivalent electron circuit used to fit the impedance spectra showed in Fig. 2, in which R_s is the solution resistance, Q_{PbSO_4} and R_{PbSO_4} are related to the capacitance and resistance of $PbSO_4$ layer, $Q_{Pb(II)}$ and $R_{Pb(II)}$ are corresponding to the capacitance and resistance of $Pb(II)$ compounds (PbO , $PbSO_4 \cdot PbO$, $PbSO_4 \cdot 3PbO$ layers, Q_{PbO} and R_{PbO} represent the capacitance and resistance of the PbO film, respectively.

motor at a scan rate of 5 nm s^{-1} , auxiliary focusing lenses are used to raise the intensity of photons toward the monochromator.

3. Results and discussions

3.1. EIS analysis of the anodic films on PbSm and PbY alloys

3.1.1. EIS of the anodic films on PbSm and PbY alloys at 1.28 V

The EIS of the anodic films on Pb and PbSm alloys at 1.28 V for 3 h in $4.5 \text{ mol L}^{-1} \text{ H}_2\text{SO}_4$ solution are showed in Fig. 1, it can be seen that two capacitive arcs appear in the Nyquist plots, in which semicircle of the arc corresponding to the frequency range of 100 KHz and 100 Hz increases with the increment of Sm, while the semicircle of the arc sharply decreases within the range from 1 Hz to 5 mHz. Two frequency regions can be observed in the corresponding bode plot (Fig. 1b), which is clearly pointed to the response of two different frequency-dependent processes with corresponding time constants, one constant time which appears in the frequency region higher than 100 Hz, the phase angle increases with the increment of Sm. However, the phase angle sharply decreases with increasing Sm in the frequency region lower than 100 Hz. According to Pavlov [3], lead electrode presents the structure of $Pb/Pb(II)(PbO, PbO \cdot PbSO_4, 3PbO \cdot PbSO_4, \text{ etc})/PbSO_4/\text{electrolyte}$ on its surface when the formation potential is close to 1.28 V. Hence, the anodic film on lead electrode at 1.28 V can be deemed as the trilaminar structure, in which the inner layer is mainly consisted of PbO , the middle layer is consisted of $Pb(II)(PbO \cdot PbSO_4, 3PbO \cdot PbSO_4, \text{ etc})$ compounds, and $PbSO_4$ is the outer layer. As $PbSO_4$ is insoluble and semi-permeable, H_2O , OH^- and H^+ ions can penetrate $PbSO_4$ film, therefore, the capacitive arc appeared in the frequency region higher than 100 Hz can be deemed as the formation of $Pb(II)$ film, and the frequency region lower than 100 Hz can be related to PbO film. The decreased phase angle with the increment of Sm content in the frequency region lower than 100 Hz implies the inhibited growth of PbO . Based on the above discussions, the equivalent electron circuit showed in Fig. 3 is used to fit the impedance spectra, a constant phase element (CPE) is

employed to study the dispersion of the system. The impedance and admittance of the CPE can be obtained with the following relationship [19,20]:

$$Z_{CPE} = [Y_0 (j\omega)^n]^{-1} \quad (1)$$

$$Y_{CPE} = Y_0 (j\omega)^n \quad (2)$$

Where j is the imaginary number, and ω is the frequency of the alternative current. The exponent, n , is defined as the CPE power, which is adjusted between 0 and 1. For $n = 1$, the CPE describes an ideal capacitor with Y_0 equal to the capacitance C . For $n = 0$, the CPE is an ideal resistor. When $n = 0.5$, the CPE represents the Warburg impedance with diffusion character. The CPE has the properties of a capacitance when $0.5 < n < 1$. The CPE describes the frequency dispersion of the time constants due to local inhomogeneity, porosity and roughness of the electrode surface.

The fitted results are showed in Table 1, the values of Y_{PbSO_4} and $Y_{Pb(II)}$ decrease, the values of R_{PbSO_4} and $R_{Pb(II)}$ increase with increasing Sm. While for Y_{PbO} and R_{PbO} , their variations are inverse to that of $Y_{PbSO_4}/Y_{Pb(II)}$ and $R_{PbSO_4}/R_{Pb(II)}$ with Sm. The increased $R_{PbSO_4}/R_{Pb(II)}$ and the decreased $Y_{PbSO_4}/Y_{Pb(II)}$ indicate the promoted growth of $PbSO_4/Pb(II)$ by addition of Sm, while the decreased R_{PbO} and the increased Y_{PbO} imply the inhibited growth of PbO in the anodic film.

As PbO has quite high resistance (about $10^{11} \Omega \text{ cm}^2$) [21], the sharply decreased resistance of PbO with increasing Sm can be beneficial to the conductivity of the anodic film on lead electrode at 1.28 V. Additionally, 1.28 V is close to the potential of the positive grid after cycle-recycle process, therefore, it can be concluded that the addition of Sm can improve the charge–discharge property of the lead acid battery.

The similar impedance spectra of the anodic film on Pb and PbY alloys at 1.28 V for 3 h in $4.5 \text{ mol L}^{-1} \text{ H}_2\text{SO}_4$ solution, are showed in Fig. 2. The Nyquist plots also display two capacitive arcs, and the semicircle within the frequency range from 100 KHz to 100 Hz increases with the increment of Y, while the semicircle of the arc sharply decreases within the range from 1 Hz to 5 mHz. The corresponding bode plots showed in Fig. 2b appear two frequency regions, the phase angle decreases in the frequency region lower 100 Hz and it decreases above 100 Hz, it is an indication of the decreased resistance of the anodic film with Y. According to the structure of the anodic film on lead alloy at 1.28 V illustrated by Pavlov [3] and the measured EIS, the equivalent electron circuit showed in Fig. 3 is employed to calculate the impedance spectra, the results are showed in Table 1, it evidently shows that the resistance of PbO film (R_{PbO}) decreases and the value of Y_{PbO} increases with Y, it implies that the growth of PbO in the anodic film is inhibited by the addition of Y. Similarly, other parameters such as Y_{PbSO_4} , $Y_{Pb(II)}$, R_{PbSO_4} and $R_{Pb(II)}$, their variations are consistent

Table 1

The fitted results of the impedance spectra of the anodic films on Pb, PbSm and PbY alloys at 1.28 V for 3 h in $4.5 \text{ mol L}^{-1} \text{ H}_2\text{SO}_4$ solution.

Elements	Pb	Pb0.019Sm	Pb0.048Sm	Pb0.097Sm	Pb0.018Y	Pb0.047Y	Pb0.095Y
$R_s/\Omega \text{ cm}^2$	0.3233	0.3232	0.2087	0.2302	0.3518	0.3675	0.2184
$Y_{PbSO_4}/\Omega^{-1} \text{ s}^n$	7.957E-5	7.783E-5	1.894E-5	1.19E-5	5.464E-5	1.514E-5	1.168E-5
n_{PbSO_4}	0.8213	0.8442	1	0.7875	0.6772	0.757	0.6257
$R_{PbSO_4}/\Omega \text{ cm}^2$	14.71	17.38	71.7	141.5	22.91	41.42	46.71
$Y_{Pb(II)}/\Omega^{-1} \text{ s}^n$	9.767E-4	2.251E-4	1.3E-4	1.24E-4	4.281E-4	1.312E-4	7.934E-5
$n_{Pb(II)}$	0.6977	0.7462	0.793	0.7216	0.8166	0.644	0.7417
$R_{Pb(II)}/\Omega \text{ cm}^2$	126.5	65.71	3376	1452	22.61	48	79.87
$Y_{PbO}/\Omega^{-1} \text{ s}^n$	1.74E-4	8.928E-4	2.432E-5	5.981E-4	3.65E-4	4.578E-4	2.092E-4
n_{PbO}	0.6859	0.6695	0.8131	0.6676	0.6466	0.6815	1
$R_{PbO}/\Omega \text{ cm}^2$	1.587E4	1.579E4	1.188E4	8055	1.311E4	1.213E4	8840
$\Sigma\chi^2$	3.82E-3	6.824E-3	1.498E-2	3.776E-3	2.312E-3	1.6E-3	3.297E-3

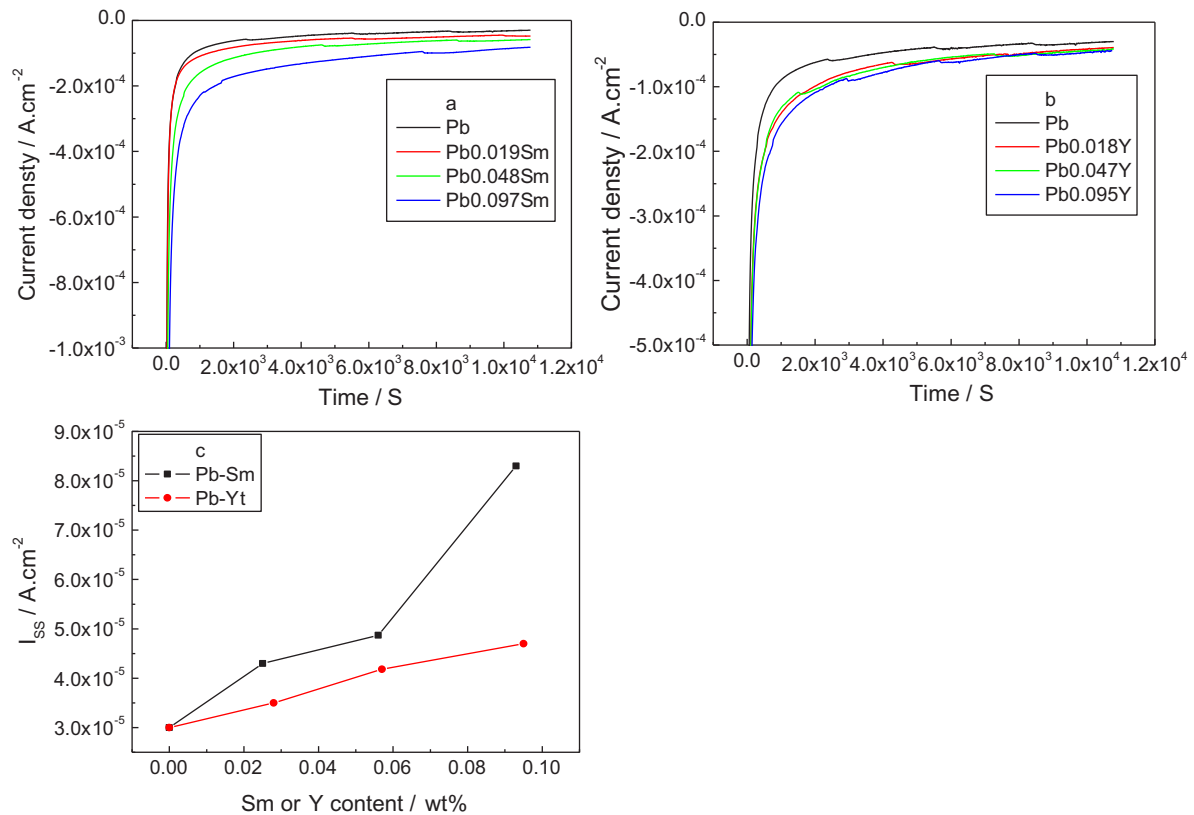


Fig. 4. The variations of current density and formation time during the formation of the anodic films on Pb, PbSm and PbY alloys at 1.28 V for 3 h in 4.5 mol L⁻¹ H₂SO₄ solution, a) Pb and PbSm alloys; b) Pb and PbY alloys; c) steady passive current density verse Sm and Y content plot.

with the variations of Y_{PbSO_4} , $Y_{Pb(II)}$, R_{PbSO_4} and $R_{Pb(II)}$ in the case of Sm. Then, we can also obtain that Y may improve the charge–discharge behavior of lead acid battery via inhibiting the growth of PbO film.

In order to better understand the influences of Sm and Y on the electron properties of the anodic films on lead electrode at 1.28 V, the current densities during the formation of the anodic film are recorded in Fig. 4, it can be seen that the current densities in the steady-passive state increase with the increment of Sm and Y, which implying the enhanced conductivity of the anodic film with the addition of Sm and Y, it is in accordance with the EIS result.

3.1.2. EIS of the anodic films on PbSm and PbY alloys at 1.5 V

As illustrated above, the conductivity of the anodic film on lead electrode at 1.28 V is very vital to the charging–discharging process of the lead acid battery. While for the anodic films formed above 1.28 V, their electron properties are also important to the charging–discharging process of the lead acid battery because these high potentials are corresponding to the potentials of the positive electrode during overcharging. It is reported by Pavlov [3] that PbO₂ is the main component of the anodic film when the potential is above 1.28 V, the positive grid can display the system of lead substrate/PbO₂/PbO₂ active material in an actual lead acid battery. The PbO₂ tends to form in the outer portion of the corrosion film, and during

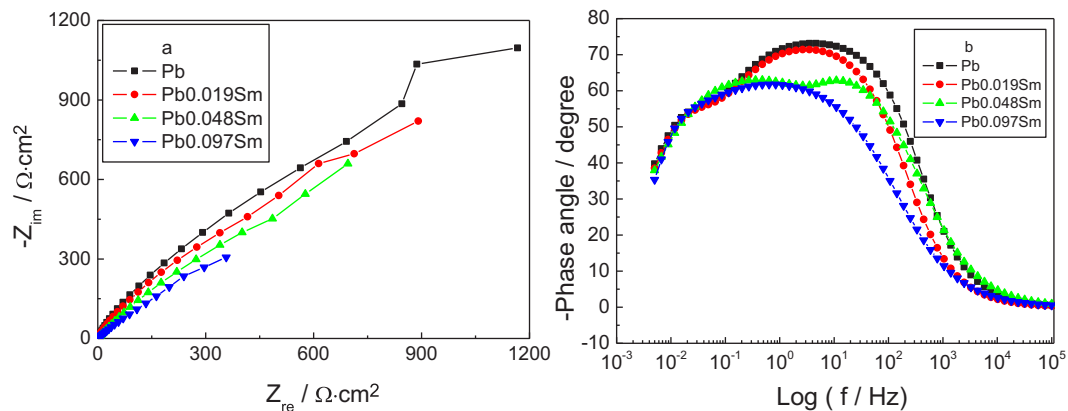


Fig. 5. EIS of the anodic films on Pb and PbSm alloys at 1.5 V for 3 h in 4.5 mol L⁻¹ H₂SO₄ solution, a) Nyquist plot; b) corresponding Bode phase angle.

discharge, this material is the last to be reduced because of its low surface area. Therefore, the investigation on the electron behavior of PbO_2 is necessary.

The EIS of the anodic films on Pb, PbSm and PbY alloys at 1.5 V for 3 h in $4.5 \text{ mol L}^{-1} \text{ H}_2\text{SO}_4$ solution are showed in Fig. 5 and Fig. 6, respectively. It can be seen that the Nyquist plots of the anodic films on PbSm and PbY alloys display the similar feature, i.e., the Nyquist plots are all consisted of two capacitive arcs, two phase angle peaks can be observed in the bode plots (Fig. 5b and Fig. 6b). The two phase angle peaks are corresponding to two time constants, one constant time appeared in the frequency region higher than 10 Hz is related to the double layer, and the other phase angle peak is corresponding to the formation of PbO_2 . Additionally, Fig. 5a and Fig. 6a show that the semicircles of the capacitive arcs decreases with the increasing Sm or Y, the corresponding bode plots (Fig. 5a and Fig. 6a) reveal that the phase angles decrease with Sm or Y, it indicates that the addition of Sm or Y may decrease the resistance of the anodic film on lead electrode at 1.5 V.

Since the lead electrode appears the Pb/ PbO_2 system at 1.5 V in sulfuric acid solution, the equivalent electron circuit showed in Fig. 7 is used to fit the impedance spectra, a constant phase element (CPE) is also employed to study the dispersion of the system. The fitted results are showed in Table 2, it can be noticed that the values of Y_{PbO_2} increases, the resistance of PbO_2 decreases with increasing Sm or Y. The decreased R_{PbO_2} and the increased Y_{PbO_2} imply the conductivity of the anodic film on lead electrode at 1.5 V is enhanced by the addition of Sm or Y.

3.1.3. EIS of the anodic films on PbSm and PbY alloys at 1.8 V

The structure of lead electrode is dependent on the potential, Pavlov [3] summarized that four electrode systems are presented depends on the applied potential in sulfuric acid: from -0.57 to -0.02 V (vs. SCE), the Pb/ PbSO_4 electrode is formed; from -0.02 to $+1.33 \text{ V}$ (vs. SCE), the Pb/ PbO / PbSO_4 electrode; and above $+1.33 \text{ V}$ (vs. SCE), the Pb/ PbO_2 electrode. While Bullock [22] provided the fourth type of electrode, Pb/t-PbO/ PbO_2 , which forms when lead is anodized in sulfuric acid solution at potentials of 1.73 V (vs. SCE) and above.

The EIS of the anodic films on PbSm and PbY alloys at 1.8 V for 3 h in $4.5 \text{ mol L}^{-1} \text{ H}_2\text{SO}_4$ solution are depicted in Fig. 8 and Fig. 9, respectively. The Nyquist plots showed in Figs. 8 and 9 present two depressed semicircles with the addition of Sm or Y, the corresponding bode plots showed in Fig. 8a and b display two phase angle peaks. Similar to the anodic films on PbSm or PbY alloys at 1.5 V, the two phase angle peaks are related to two time constants. The depressed semicircle and phase angle with Sm or Y indicate the decreased resistance of Pb(II) and Pb(IV) films. According to Bullock

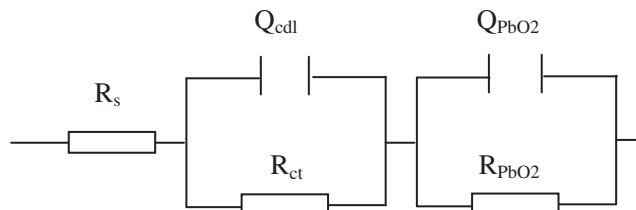


Fig. 7. The equivalent electron circuit used to fit the impedance spectra showed in Figs. 5 and 6, in which R_s is the solution resistance, Q_{cdl} and R_{ct} represent the capacitance and resistance of the double layer, $Q_{\text{Pb(IV)}}$ and $R_{\text{Pb(IV)}}$ are corresponding to the capacitance and resistance of PbO_2 layers, respectively.

[22], the outer PbO_2 inhibits the ionic diffusion, the formation of the fourth electrode system is controlled by the diffusion process, therefore, the equivalent electron circuit showed in Fig. 10 is used to fit the impedance spectra. In this equivalent electron circuit, Z_w is the diffusion impedance, it is usually depicted as Y_w , which value is direct to the square value of the diffusion coefficient D . Table 3 shows the fitted results, it can be noticed that the values of $Y_{\text{PbO}/\text{PbO}_2}$ increases, the resistance of the anodic film ($R_{\text{PbO}/\text{PbO}_2}$) decreases with increasing Sm or Y content. The decreased film resistance and the increased $Y_{\text{PbO}/\text{PbO}_2}$ imply the conductivity of the anodic film on lead electrode at 1.8 V is enhanced by the addition of Sm or Y. While for Y_w , the value of Y_w increases with Sm or Y, it implies that the ionic diffusion is increased. In other words, the growth of PbO in the anodic film formed above 1.73 V is hindered by the addition of Sm or Y.

3.2. Galvanostatic anodic polarization curves of Pb, PbSm and PbY alloys in $4.5 \text{ mol L}^{-1} \text{ H}_2\text{SO}_4$

The galvanostatic anodic polarization curves of Pb and PbSm electrodes in $4.5 \text{ mol L}^{-1} \text{ H}_2\text{SO}_4$ solution at 25°C applying various current densities are studied in Fig. 11, it shows that the general anodic behaviors of four electrodes are similar, there is a rapid and almost linear change of potential (region a), the duration time of this process is defined as τ . After the region a, the electrode acquires a steady-state potential, arrest a^* . The potential along this arrest (region a^*) remains constant and does not change appreciably, it is related to the formation of the anodic film on lead electrode. The initial potential of region a is defined as the dissolution potential, $E_{\text{dissolution}}$, similarly, the initial potential of region a^* is defined as the passivation potential, $E_{\text{passivation}}$.

Fig. 12a shows the variation of $E_{\text{passivation}}$ and the logarithm of the imposed current densities, i in mA cm^{-2} . It is clear that as the

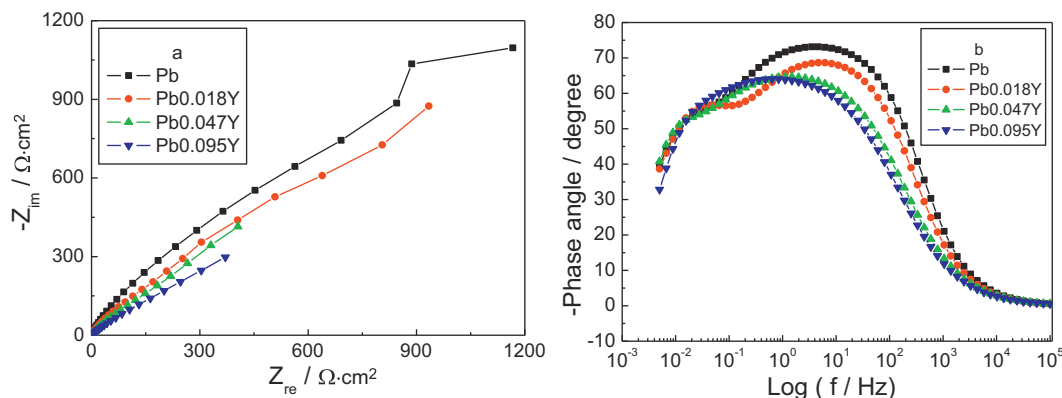


Fig. 6. EIS of the anodic films on Pb and PbY alloys at 1.5 V for 3 h in $4.5 \text{ mol L}^{-1} \text{ H}_2\text{SO}_4$ solution, a) Nyquist plot; b) corresponding Bode phase angle.

Table 2The fitted results of the impedance spectra of the anodic films on Pb, PbSm and PbY alloys at 1.5 V for 3 h in 4.5 mol L⁻¹ H₂SO₄ solution.

Elements	Pb	Pb0.019Sm	Pb0.048Sm	Pb0.097Sm	Pb0.018Y	Pb0.047Y	Pb0.095Y
$R_s/\Omega \text{ cm}^2$	0.313	0.4281	0.3112	0.3753	0.4077	0.3112	0.276
$Y_{cdl}/\Omega^{-1} \text{ S}^n$	9.246E-3	0.0115	0.01023	0.02576	0.01157	0.01932	0.03025
n_{cdl}	0.8357	0.8353	0.7358	0.6848	0.8373	0.7146	0.7
$R_{ct}/\Omega \text{ cm}^2$	168.1	114	139.3	154.5	79.41	176.4	131.3
$Y_{PbO_2}/\Omega^{-1} \text{ S}^n$	8.846E-3	0.01239	0.02311	0.07573	0.01041	0.06563	0.0744
n_{PbO_2}	0.8432	0.8264	1	1	0.7916	1	1
$R_{PbO_2}/\Omega \text{ cm}^2$	2676	1904	1625	403.8	1827	615.3	356.4
$\Sigma\chi^2$	1.164E-2	8.6E-3	1.726E-3	2.98E-2	8.615E-3	3.9E-3	2.98E-3

imposed current densities increases, $E_{\text{passivation}}$ shifts to more positive values according to the empirical reaction:

$$E_{\text{passivation}} = \alpha + \beta \lg i \quad (3)$$

Where α is a constant, β is the slope of $E_{\text{passivation}}$ verse $\lg i$ plot. It can be obtained that the fitted slopes β/mV are 172.98, 174.8, 220.8 and 231.7 in the case of Pb, Pb0.018Sm, Pb0.049Sm and Pb0.095Sm electrodes, respectively. Apparently, the slope β increases with the increment of Sm, this result indicates that the passivation potential of PbCaSn alloy in H₂SO₄ solution moves to positive direction with the addition of Sm.

Similarly, $E_{\text{dissolution}}$ and the logarithm of the imposed current densities appear the linear relationship, the result is showed in Fig. 12b, and the fitted slopes are 27.95, 29.17, 40.24 and 43.39, respectively. Obviously, the fitted slope decreases with the

increment of Sm, it can be concluded from this result that the initial passive potential of PbCaSn alloy in H₂SO₄ solution shifts to positive direction with Sm, which implying the enhanced passivity of PbCaSn alloy with the addition of Sm.

Finally, Fig. 12c gives the variation of $\text{Log}\tau$ and $\text{Log}i$, it can be seen that $\text{Log}\tau$ is dependent linearly on $\text{Log}i$, the slopes of the linear plots in the case of PbCaSn electrode, PbCaSn0.018Sm, PbCaSn0.049Sm and PbCaSn0.079Sm electrodes are -1.5855, -1.4878, -1.484 and -1.4455 respectively. This value indicates that the diffusion of ions through the passivation process becomes the controlling step [23,24]. The decreased slope with the increment of Sm indicates the decreased duration time of passive process of PbCaSn alloy in 4.5 mol L⁻¹ H₂SO₄ solution.

For Pb and PbY alloys, the galvanostatic anodic polarization curves of two electrodes are depicted in Fig. 13, the feature of the polarization curve is similar to that of the polarization curve

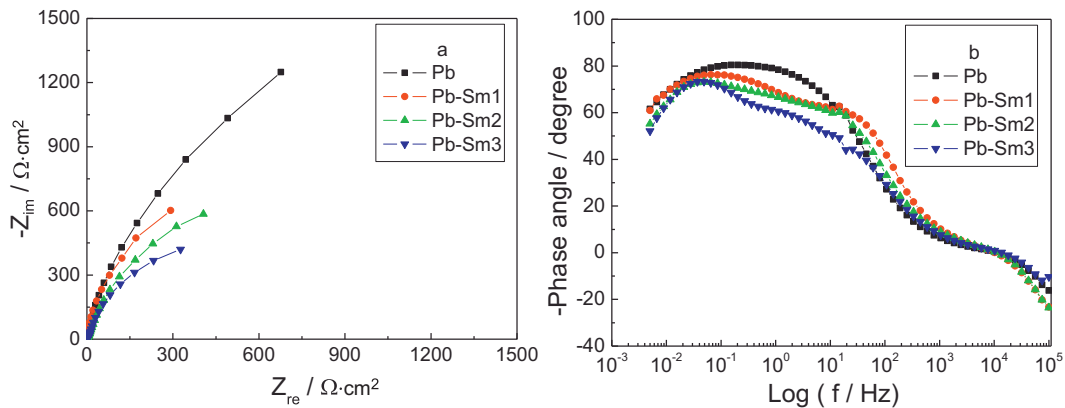


Fig. 8. EIS of the anodic films on Pb and PbSm alloys at 1.8 V for 3 h in 4.5 mol L⁻¹ H₂SO₄ solution, a) Nyquist plot; b) corresponding Bode phase angle.

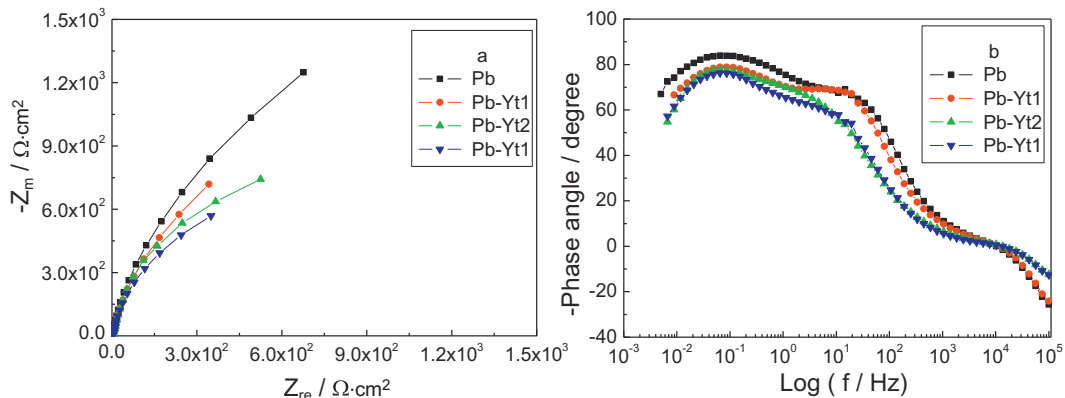


Fig. 9. EIS of the anodic films on Pb and PbY alloys at 1.8 V for 3 h in 4.5 mol L⁻¹ H₂SO₄ solution, a) Nyquist plot; b) corresponding Bode phase angle.

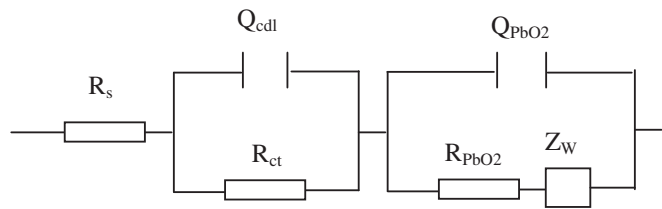


Fig. 10. The equivalent electron circuit used to fit the impedance spectra showed in Figs. 8 and 9, in which R_s is the solution resistance, Q_{cdl} and R_{ct} represent the capacitance and resistance of the double layer, Q_{PbO_2} and R_{PbO_2} are corresponding to the capacitance and resistance of PbO_2 layers, respectively.

showed in Fig. 11. Based on Eq. (3), Fig. 14a shows the slopes of the linear $E_{passivation}$ versus $\text{Log} i$ plots in the case of Pb, Pb0.018Y, Pb0.049Y and Pb0.095Y electrodes, which are 172.98, 183.7, 235 and 331.8, respectively. The slopes of the linear $E_{dissolution}$ versus $\text{Log} i$ plots showed in Fig. 14b are 172.98, 183.7, 235 and 331.8 in the case

of Pb, Pb0.018Y, Pb0.049Y and Pb0.095Y electrodes, and the slopes of the linear $\text{Log} \tau$ versus $\text{Log} i$ plots are -1.5855 , -1.5812 , -1.5658 and -1.5481 , respectively. Apparently, the addition of Y may improve the passivity of Pb in sulfuric acid solution.

3.3. Mott–Schottky analysis of the anodic films

The semi-conductive property of the passive film on metal or alloy is usually evaluated by measuring the electrode capacitance as a function of the potential (E). The Mott–Schottky plot expresses the relationship of space charge capacitance C_{sc} , of a n -type semi-conductor and the film-formation potential E as following [25,26]:

$$C^{-2} = C_{sc}^{-2} = \frac{2}{\epsilon \epsilon_0 e N_D} \left(E - E_{FB} - \frac{KT}{e} \right) \tag{4}$$

Where ϵ is the dielectric constant of the passive film, ϵ_0 is the vacuum permittivity ($8.854 \times 10^{-14} \text{ F cm}^{-1}$), e is the electron charge,

Table 3
The fitted results of the impedance spectra of the anodic films on Pb, PbSm and PbY alloys at 1.8 V for 3 h in 4.5 mol L⁻¹ H₂SO₄ solution.

Elements	Pb	Pb0.019Sm	Pb0.048Sm	Pb0.097Sm	Pb0.018Y	Pb0.047Y	Pb0.095Y
$R_s/\Omega \text{ cm}^2$	0.3955	0.352	0.3191	0.398	0.2835	0.4761	0.4214
$Y_{cdl}/\Omega^{-1} \text{ S}^n$	0.04828	0.01713	0.0349	0.04477	0.02578	0.04262	0.03989
n_{cdl}	0.7327	0.809	0.7304	0.66	0.8052	0.6937	0.7422
$R_{ct}/\Omega \text{ cm}^2$	147.5	7.736	17.39	17.07	9.539	11.86	9.7
$Y_{PbO/PbO_2}/\Omega^{-1} \text{ S}^n$	0.00834	0.0185	0.02773	0.04241	0.0159	0.02568	0.03545
n_{PbO/PbO_2}	0.945	0.9231	0.9012	0.9235	0.791	0.8756	0.9124
$R_{PbO/PbO_2}/\Omega \text{ cm}^2$	3003	1810	1615.8	617.8	1503	801.1	714
$Y_w/\Omega^{-1} \text{ S}^{-0.5}$	0.004435	0.007143	0.008358	0.02052	0.005276	0.006898	0.008257
$\Sigma \chi^2$	4.819e-3	1.376e-2	1.158e-2	3.54e-3	1.22e-2	3.137e-3	3.256e-3

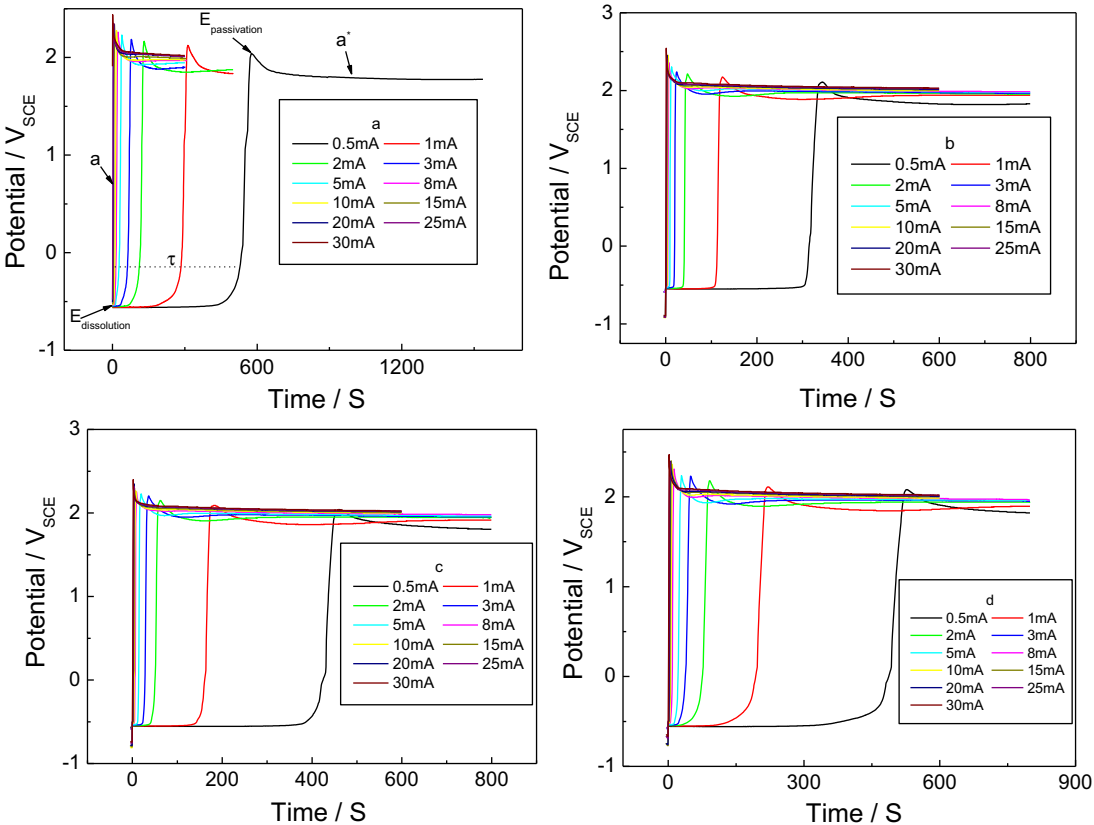


Fig. 11. Anodic polarization curves of four electrodes in 4.5 mol L⁻¹ H₂SO₄ solution at 25 °C with different current densities, a) 0%Sm, b) 0.019%Sm, c) 0.048%Sm, d) 0.079%Sm.

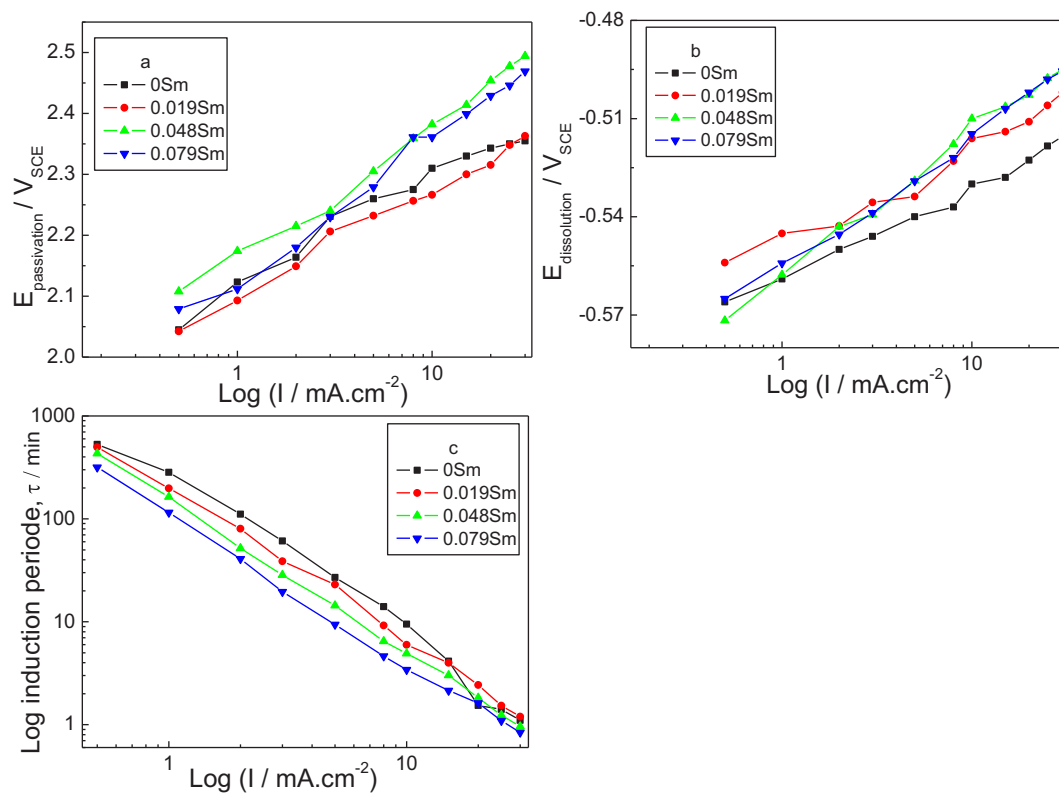


Fig. 12. Variation of (a) the passivation potential arrest, $E_{\text{passivation}}$, (b) the dissolution potential arrest, $E_{\text{dissolution}}$, and (c) the duration time of the dissolution arrest, τ with imposed current densities, $T = 25 \pm 0.5$ °C.

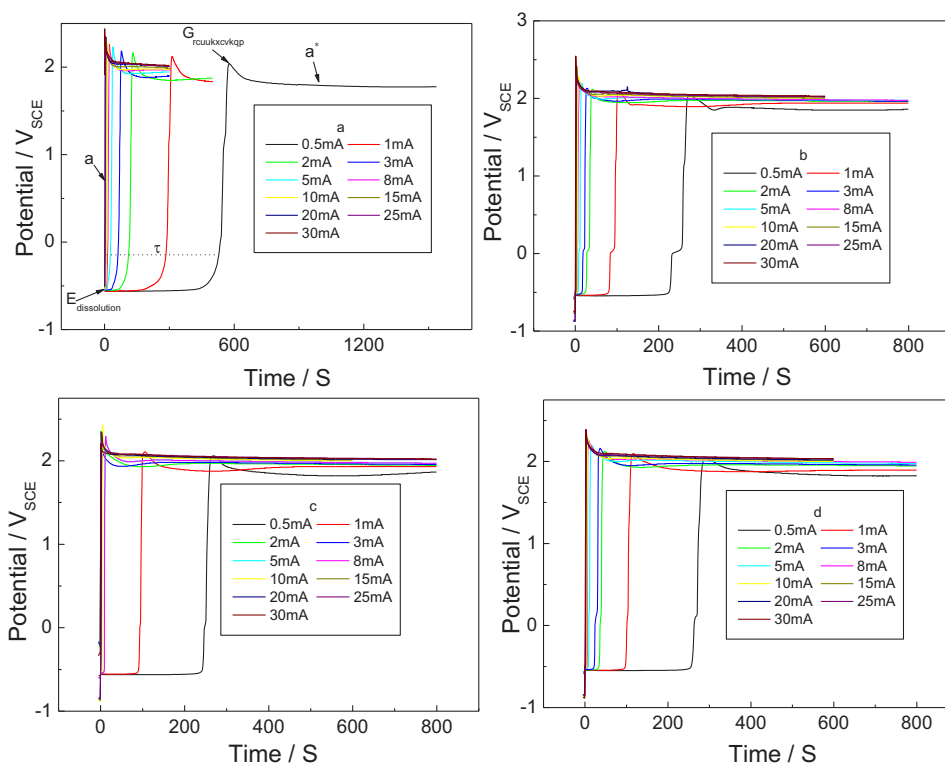


Fig. 13. Anodic polarization curves of four electrodes in 4.5 mol L⁻¹ H₂SO₄ solution at 25 °C with different current densities, a) 0%Y, b) 0.019%Y, c) 0.048%Y, d) 0.079%Y.

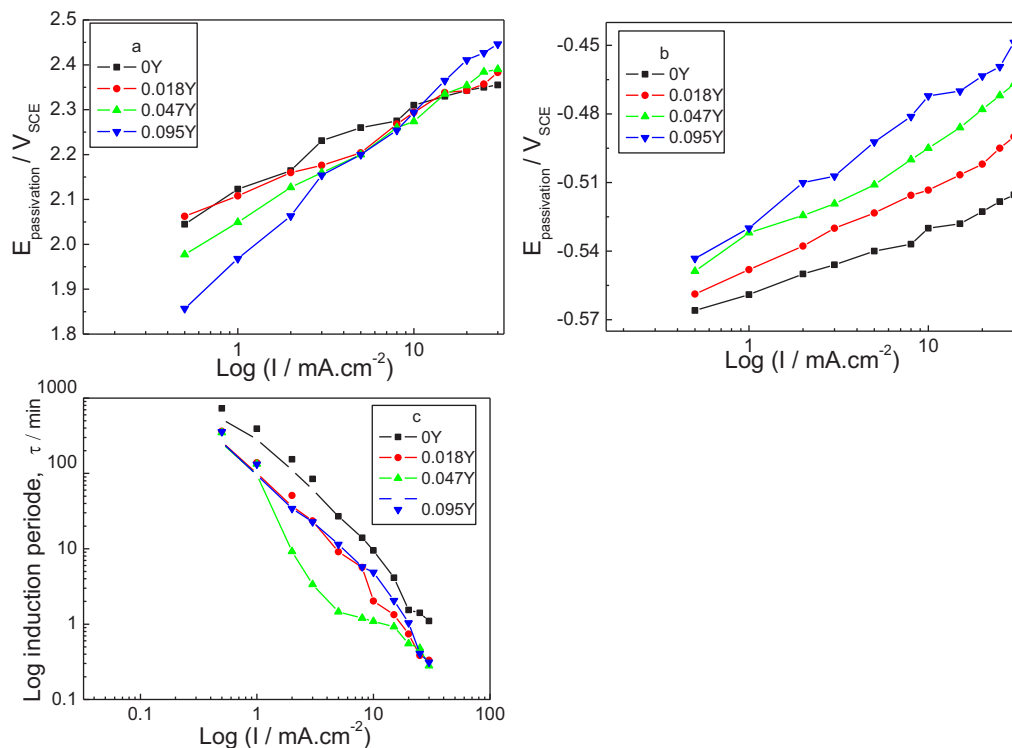


Fig. 14. Variation of (a) the passivation potential arrest, $E_{\text{passivation}}$, (b) the dissolution potential arrest, $E_{\text{passivation}}$, and (c) the duration time of the dissolution arrest, τ with imposed current densities, $T = 25 \pm 0.5$ °C.

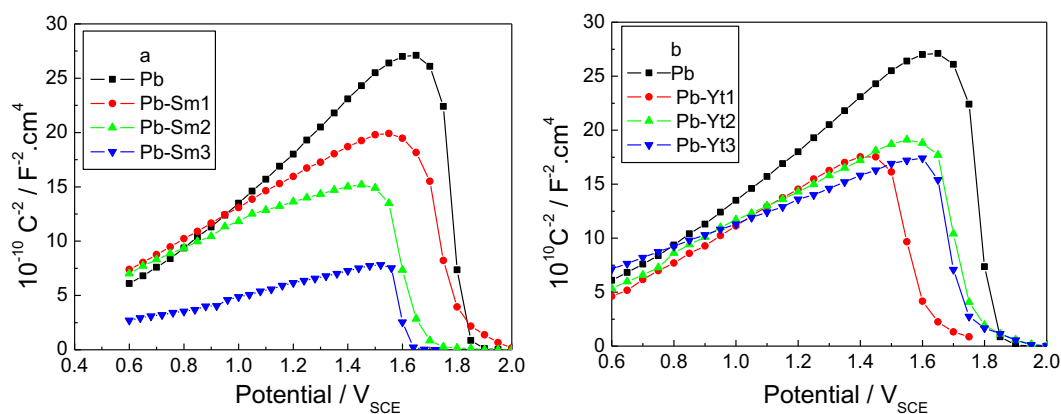


Fig. 15. The Mott–Shottky plots of the anodic films on Pb, PbSm, and PbY alloys at 1.28 V for 3 h in 4.5 mol L^{-1} H_2SO_4 solution, a) Pb and PbSm alloy; b) Pb and PbY alloy.

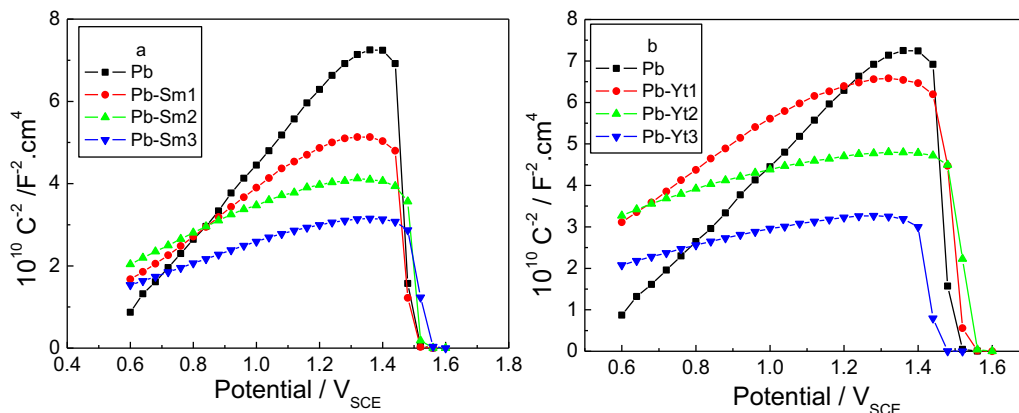


Fig. 16. The Mott–Shottky plots of the anodic films on Pb, PbSm, and PbY alloys at 1.5 V for 3 h in 4.5 mol L^{-1} H_2SO_4 solution, a) Pb and PbSm alloy; b) Pb and PbY alloy.

N_D is the donor density. E_{FB} is the flat-band potential, K is the Boltzmann constant, T is the absolute temperature. N_D can be estimated from the slope of linear fitted M–S plots, while E_{FB} comes from the extrapolation for $C_{sc}^{-2} = 0$.

The Mott–Schottky plots of the anodic films on Pb, PbSm and PbY alloys at 1.28 V, 1.5 V and 1.8 V for 3 h in 4.5 mol L⁻¹ H₂SO₄ solution are depicted in Fig. 15, Fig. 16 and Fig. 17, respectively. It can be seen that there is a good linear relationship between C^{-2} and sweep potential in the potential region from 0.5 V to 1.6 V, and there is no Mott–Schottky response between C^{-2} and E in this potential region of 1.5 V and 2.0 V, because the deep exhausted layer of electron falls in this potential region. The slopes of all M–S plots exhibit positive, indicating the n -type semi-conductive character, the slopes decrease with the increment of Y or Sm. According to Eq. (4), the donor density of the anodic film increases with the increment of Sm or Y, which indicating the increased point defects densities in the anodic film. As the point defect in the anodic film can behave as the charge carrier, the increased number of point defect may be beneficial to the conductivity of the anodic film, and even to improve the charge–discharge property of the lead acid battery.

For the anodic film on lead electrode at 1.28 V, the system of Pb/PbO·PbSO₄/PbSO₄ is formed, in which PbO is an oxide semi-conductor with interstitial oxygen (PbO_{1+x}) based on the crystallography of PbO, therefore, it has p -type semi-conductive character. However, the positive slopes of M–S plots meaning the n -type semi-conductive performance of the anodic film, herewith, there existing the oxides with n -type semi-conductive within the anodic film, comparing with the EIS result, PbO₂ may exist in the anodic film, and the anodic film can be deemed as the mixture of PbO and PbO₂. While PbO₂ has n -type semi-conductive character, it can explain the n -type semi-conductive behavior of the anodic films on four electrodes, it is also in accordance with Bojinov [27].

In order to accurately illustrate the semi-conductive properties of the anodic films, Table 4 lists the slopes of MS plots of the anodic films on Pb, PbSm and PbY alloys at 1.28 V, 1.5 V and 1.8 V for 3 h in 4.5 mol L⁻¹ H₂SO₄ solution, it can be seen that the slopes of the MS plots decrease with the increment of Sm or Y, which implies that the donor densities of the anodic films increase with Sm and Y, which can also be concluded that the resistances of the anodic films decrease with Sm and Y, it is in agreement with the result of EIS. Let's see Table 4 again, the slopes of the MS plots of the anodic films on PbSm or PbY alloys at 1.28 V is the highest, and the slopes in the case of 1.8 V is the middle, it indicates that the donor density in the anodic film on 1.28 V is the lowest, and the density in the case of 1.5 V is the highest. The high donor density in the anodic film

Table 4

The slopes of MS plots of the anodic films on Pb, PbSm and PbY alloys at 1.28 V, 1.5 V and 1.8 V for 3 h in 4.5 mol L⁻¹ H₂SO₄ solution.

Electrodes	1.28 V	1.5 V	1.8 V
Pb	23.37×10^{10}	8.887×10^{10}	15.673×10^{10}
Pb0.019%Sm	13.89×10^{10}	5.561×10^{10}	12.143×10^{10}
Pb0.048%Sm	10.73×10^{10}	2.292×10^{10}	8.712×10^{10}
Pb0.097%Sm	5.92×10^{10}	1.932×10^{10}	5.985×10^{10}
Pb0.018%Y	16.92×10^{10}	5.463×10^{10}	10.774×10^{10}
Pb0.047%Y	15.11×10^{10}	3.189×10^{10}	6.962×10^{10}
Pb0.095%Y	10.62×10^{10}	2.514×10^{10}	4.92×10^{10}

implies the good conductivity, therefore, it can be concluded that the anodic film on lead electrode has the best conductivity, and 1.8 V is the better, the reason may be related to the dependent film composition on the applied potential. As noted above by Pavlov [3] and Bullock [22], four following electrode systems can be formed on lead electrode: Pb/PbSO₄ (−0.57 V to −0.02 V); Pb/PbO/PbSO₄ (−0.024 V to +1.33 V); Pb/PbO₂ (above 1.33 V) and Pb/t–PbO/PbO₂ (above 1.73 V), considering the high resistance of PbO, it infers that conductivity of the anodic film on lead electrode at 1.5 V is better than that in the case of 1.8 V, this conclusion is in agreement with the MS and EIS results.

3.4. Photocurrent of the anodic films

Photo-electrochemical technique is a powerful measurement widely used to examine the in situ composition and structure of the passive films formed on metals and alloys. Fig. 18a, Fig. 19a and Fig. 20a show the variation of photocurrent, i_{ph} , and the incident wavelength with +300 mV applied potential in the cases of 1.28 V, 1.5 V and 1.8 V, respectively. It can be seen that the photocurrent increases with increasing the wavelength, the photocurrent reaches to the maximum value when the incident wavelength arrives at about 350 nm, then the photocurrent decreases with continuing to increase wavelength. The photocurrents increase with the increment of Sm or Y, the band gap E_g of the anodic film has been estimated from the photocurrent spectra according to Eq. (5) on assumption of the proportional relationship between photocurrent and the optical absorption [28]:

$$I_{ph} = \frac{A(h\nu - E_g)^n}{h\nu} \quad (5)$$

Where A is a constant, $h\nu$ the photon energy, and E_g the band gap energy, n value of 2 has been used predominantly for the passive film

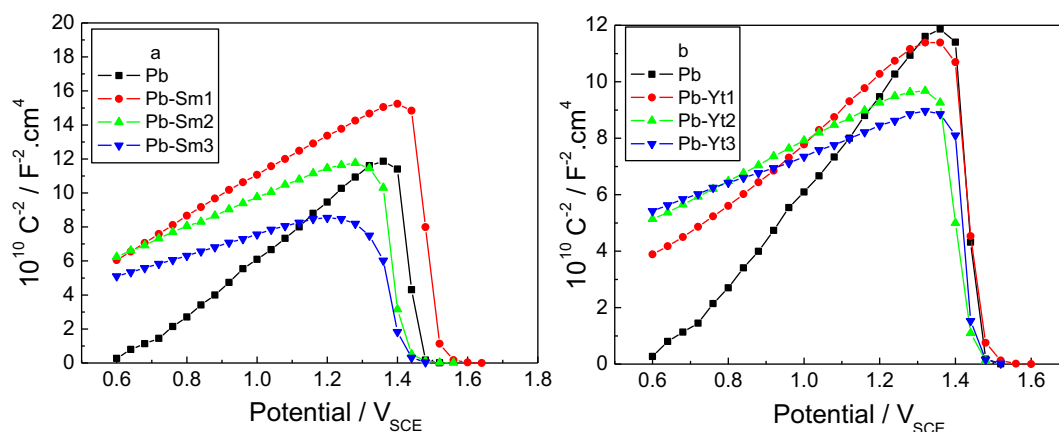


Fig. 17. The Mott–Schottky plots of the anodic films on Pb, PbSm, and PbY alloys at 1.8 V for 3 h in 4.5 mol L⁻¹ H₂SO₄ solution, a) Pb and PbSm alloy; b) Pb and PbY alloy.

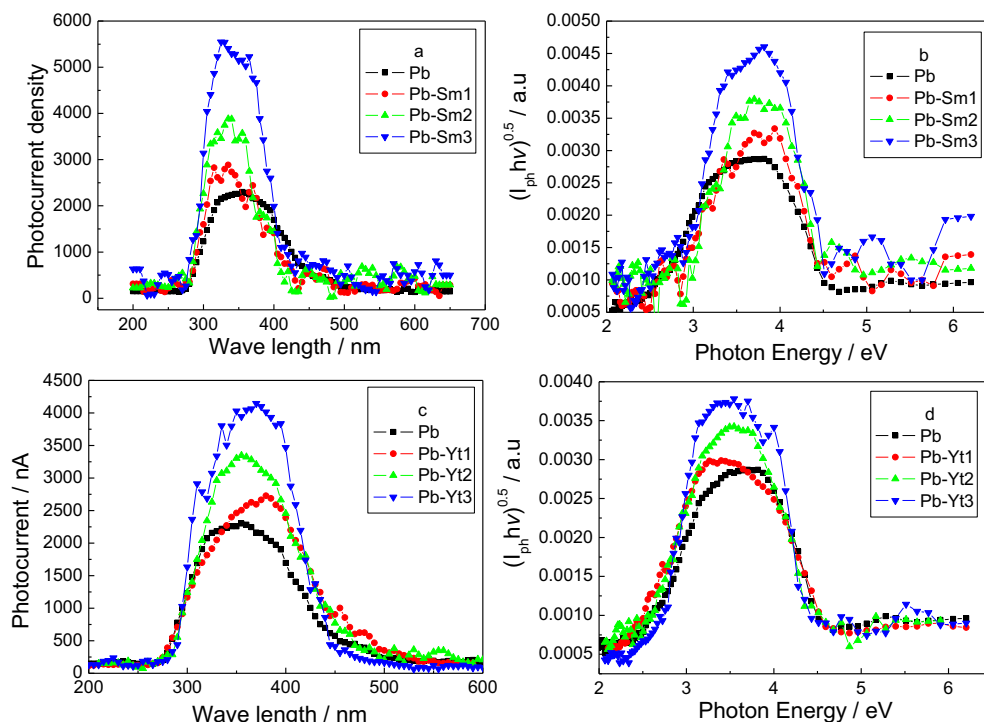


Fig. 18. The photocurrent verse wave length plot and the corresponding $(I_{ph} \cdot hv)^{0.5} \sim$ photon energy plot of the anodic films on Pb, PbSm and PbY alloys at 1.28 V for 1 h in 4.5 mol L⁻¹ H₂SO₄ solution, a) Pb and PbSm alloy, b) Pb and PbY alloy.

[28]. According to Eq. (5), Fig. 18b, Fig. 19b and Fig. 20b show the corresponding $(I_{ph} \cdot hv)^{0.5}$ -incident energy plot, the photocurrent increases with the increment of Sm or Y. According to Pavlov [29], the point defect within the anodic film can serve as the electron carrier,

the electron jumps over the bandgap and passes into the conduction band of the anodic film, and then the photocurrent occurs. The increased photocurrent implies the increases point defect in the anodic film, it is in agreement with the result of Mott–Schottky plot.

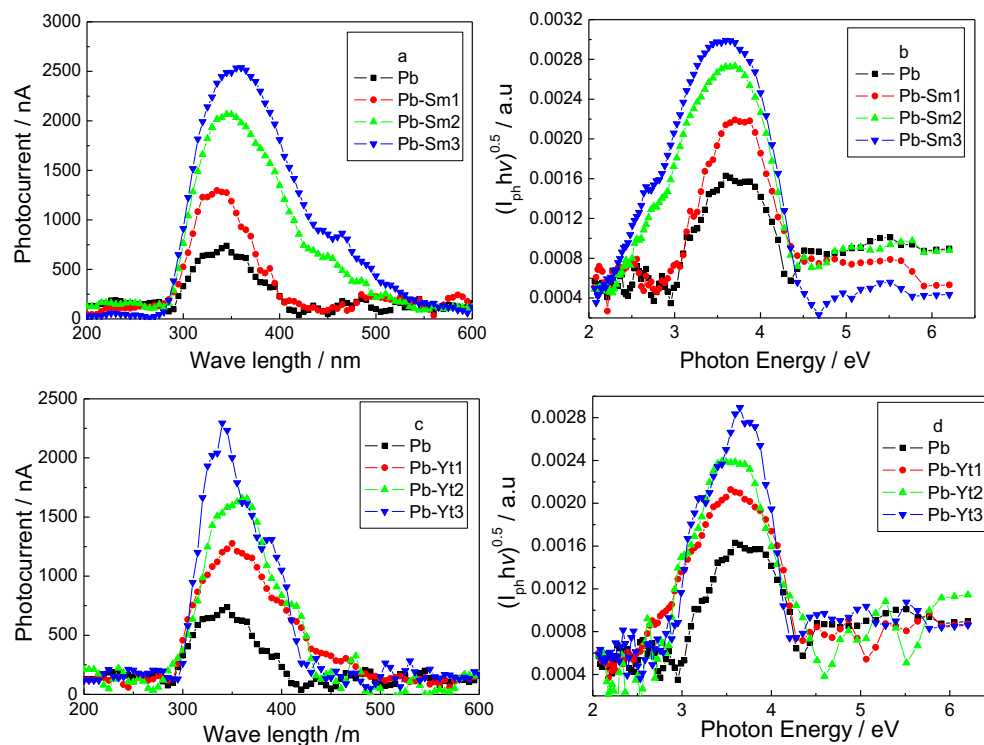


Fig. 19. The photocurrent verse wave length plot and the corresponding $(I_{ph} \cdot hv)^{0.5} \sim$ photon energy plot of the anodic films on Pb, PbSm and PbY alloys at 1.5 V for 1 h in 4.5 mol L⁻¹ H₂SO₄ solution, a) Pb and PbSm alloy, b) Pb and PbY alloy.

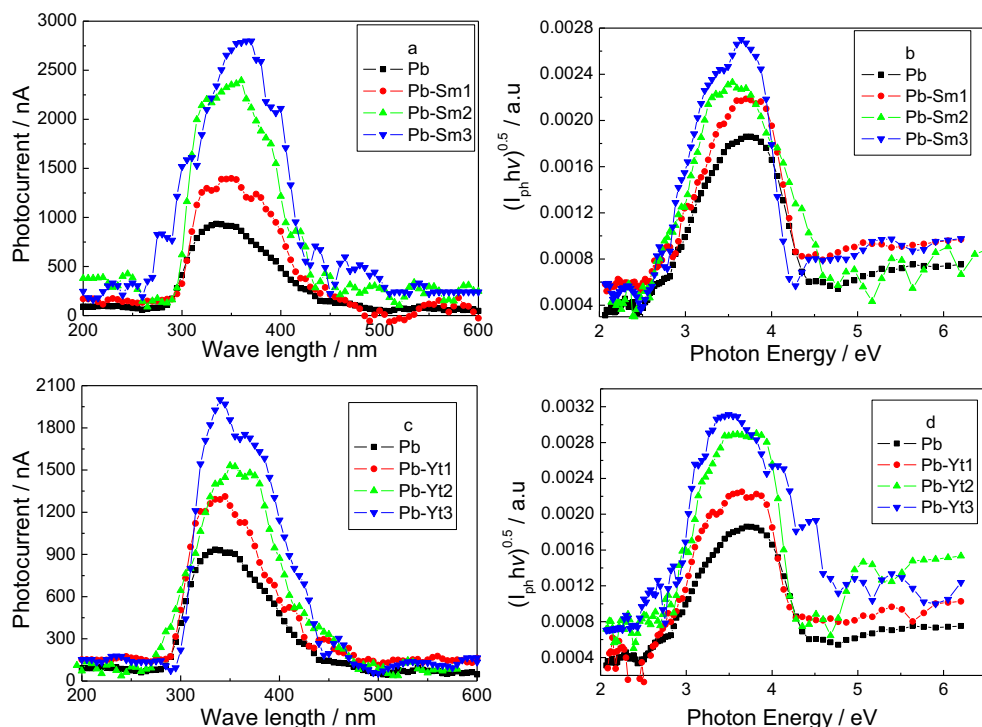


Fig. 20. The photocurrent verse wave length plot and the corresponding $(I_{ph} \cdot hv)^{0.5} \sim$ photon energy plot of the anodic films on Pb, PbSm and PbY alloys at 1.8 V for 1 h in $4.5 \text{ mol L}^{-1} \text{ H}_2\text{SO}_4$ solution, a) Pb and PbSm alloy, b) Pb and PbY alloy.

4. Conclusion

The addition of the rare earth elements Sm and Y can affect the electron properties of the anodic films on lead electrode in sulfuric acid solution. The resistance of the anodic film on lead electrode at 1.28 V is decreased, the reason is related to the inhibited growth of PbO in the anodic film by the addition of Sm or Y. The resistances of the anodic films on lead electrode at 1.5 V and 1.8 V decrease with adding Sm or Y into lead, it is related to the increased number of the point defect within the anodic films. Additionally, the addition of Sm or Y can decrease the oxygen and hydrogen evolution of lead electrode in sulfuric acid.

References

- [1] B.K. Mahato, J.L. Strebe, D.F. Wilkinson, K.R. Bullock, J. Electrochem. Soc. 123 (1985) 19–23.
- [2] N. Bui, P. Mattesco, P. Simon, J. Steinmetz, E. Rocca, J. Power Sources 67 (1997) 61–67.
- [3] D. Pavlov, C.N. Pouliev, E. Klaja, N. Iordanov, J. Electrochem. Soc. 116 (1969) 316.
- [4] J.L. Cailerie, L. Albert, J. Power Sources 67 (1997) 279–281.
- [5] D. Pavlov, J. Electrochem. Soc. 136 (1989) 27–33.
- [6] C. Brissaud, G. Reumont, J.P. Smaha, J. Foc, J. Power Sources 64 (1997) 117–122.
- [7] A.F. Hollenkamp, J. Power Sources 59 (1996) 87–98.
- [8] R. Miraglio, L. Albert, A.E.I. Ghachcham, J. Steinmetz, J.P. Hilger, J. Power Sources 53 (1995) 55–61.
- [9] E. Rocca, J. Steinmetz, S. Weber, J. Electrochem. Soc. 146 (1999) 54–58.
- [10] D. Pavlov, Electrochim. Acta 23 (1978) 845–854.
- [11] D.G. Li, G.S. Zhou, J. Zhang, M.S. Zheng, Electrochim. Acta 52 (2007) 2146.
- [12] M.L. Yan, Z.W. Zhou, J. Power Sources 195 (2010) 631.
- [13] H.T. Liu, J. Yang, H.H. Liang, J.H. Zhuang, W.F. Zhou, J. Power Sources 93 (2001) 230.
- [14] D.G. Li, J.D. Wang, D.R. Chen, J. Power Sources 210 (2012) 163.
- [15] Aiju Li, Yiman Chen, Hongyu Chen, Dong Shu, Weishan Li, Hui Wang, Chuanlong Dou, Wei Zhang, Shun Chen, J. Power Sources 189 (2009) 1204.
- [16] H.Y. Chen, S. Li, A.J. Li, D. Shu, W.S. Li, C.L. Dou, Q. Wang, G.M. Xiao, S.G. Peng, S. Chen, W. Zhang, H. Wang, J. Power Sources 168 (2007) 79.
- [17] Reza Karimi Shervedani, Asghar Zeini Isfahani, Rasool Khodavisy, Abdolhamid Hatefi-Mehrjardi, J. Power Sources 164 (2007) 890.
- [18] N.E. Bagshaw, J. Power Sources 2 (1978) 337.
- [19] K. Juttner, Electrochim. Acta 35 (1990) 1501.
- [20] V.A. Alves, M.A. Brett Christopher, Electrochim. Acta 47 (2002) 2081.
- [21] D. Pavlov, in: B.D. McNicol, D.A.J. Rand (Eds.), Power Sources for Electrical Vehicles, Elsevier, Amsterdam, 1984.
- [22] K.R. Bullock, M.A. Butter, J. Electrochem. Soc. 133 (1986) 1085.
- [23] E.E. Agd El Aal, J. Power Sources 75 (1998) 36.
- [24] E.E. Abd El Aal, Corros. Sci. 45 (2003) 641.
- [25] H.W. Wilson, J. Appl. Phys. 48 (1977) 4292.
- [26] J.F. Dewald, J. Phys. Chem. Solids 14 (1960) 155.
- [27] M. Bojinov, K. Solmi, G. Sundholm, Electrochim. Acta 39 (1994) 719.
- [28] U. Stimming, Electrochim. Acta 31 (1986) 415.
- [29] D. Pavlov, S. Zanava, G. Papazov, J. Electrochem. Soc. 124 (1977) 1522.